Geoderma 431 (2023) 116363

Contents lists available at ScienceDirect

Geoderma

journal homepage: www.elsevier.com/locate/geoderma

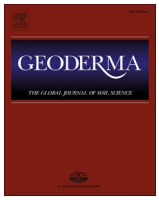

Determination of soil pore size distribution and water retention curve by internal magnetic field modulation at low field ^{1}H NMR

Etelvino Henrique Novotny [a,*], Eduardo Ribeiro deAzevedo [b], Gustavo de Godoy [c], Daniel Martelozo Consalter [d], Miguel Cooper [c]

[a] Embrapa Soils, Brazilian Agricultural Research Corporation – Embrapa, Rio de Janeiro – RJ, Brazil
[b] São Carlos Institute of Physics, University of São Paulo, São Carlos – SP, Brazil
[c] Luiz de Queiroz School of Agriculture, University of São Paulo, Piracicaba – SP, Brazil
[d] Fine Instrument Technology, São Carlos – SP, Brazil

ARTICLE INFO

Handling Editor: Morgan Cristine L.S.

Keywords:
Pore length scales
Soil water retention
Diffusion eigenmode detection
DDIF

ABSTRACT

The determination of the soil pore size distribution, water retention curve, and derived parameters that control important processes in soils, such as water supply for plants; infiltration; water and solute movement in soils; erosion; plant nutrients and contaminants transport, etc, are challenging and the available methods are expensive, time-consuming and prone to bias and errors. The use of ^{1}H Nuclear Magnetic Resonance (NMR) relaxometry to characterise the soil porosity and hydraulic properties through spin-lattice and spin-spin relaxometry results in an ill-posed problem with two correlated unknown quantities: the pore length scales, and surface relaxivity. To overcome this limitation of NMR relaxometry, we propose the use of a method that directly accesses the NMR diffusion modes governed only by the pore size, and therefore, independent of the unknown surface relaxivity. The manuscript describes an unprecedent application in Soil Science of the Decay due to Diffusion in Internal Field (DDIF) method to successfully determine the pore size distribution of undisturbed soil samples, as well as to estimate the water retention curves from the pore size distribution.

1. Introduction

Pore size distribution and the soil water retention curve (SWRC) are key properties of soils and essential for the understanding of fluid and solute transport rates within the vadose zone with a wide range of applications such as agriculture, forestry, ecology, environmental sciences and civil engineering (Stingaciu et al., 2010). These hydrophysical properties influence soil infiltration rates; runoff and erosion processes; plant growth; microbiota development; plant nutrients and contaminants transport; as well as the recharge of aquifers and discharge to surface waters (Nimmo, 2009; Wang et al., 2015; Medici et al., 2019; Villarreal et al., 2020). However, the quantification of soil hydraulic properties is challenging (Costabel and Hiller, 2021) and the conventional empirically-based SWRC determination methods (e.g.: a combination of porous plate and pressure cell or multistep outflow) are dependent on laborious, expensive and time-consuming procedures (Rieu and Sposito, 1991; Sun et al., 2020).

The main limitation is related to the long time needed for the samples to reach the hydrostatic equilibrium, which takes from days to several months (Hunt and Ewing, 2009). Furthermore, this laborious methodology is susceptible to errors, especially at low matric potentials, such as the loss of hydraulic contact between the samples and pressure plates, and the uncertainty in the determination of the hydrostatic equilibrium (Campbell et al., 2007; Solone et al., 2012). These difficulties have instigated researchers to search for new methodologies to determine and predict the SWRC.

Using time-domain nuclear magnetic resonance (TD-NMR) to determine the porosity and pore size distribution of rocks (Benavides et al., 2020) as well as soil porosity and soil hydraulic properties is a current challenge (Sucre et al., 2011; Dlugosch et al., 2013; Costabel and Yaramanci, 2013; Costabel et al., 2018; Knight et al., 2016; Costabel and Hiller, 2021). The current approach uses fluid ^{1}H relaxivity-dependent ground mode, i.e., relaxation mode (Song, 2003) (T_1: spin-lattice or longitudinal relaxation and T_2: spin-spin or transversal relaxation), or a combination of both relaxation processes (Jaeger et al., 2009; Benavides et al., 2020). However, these relaxation processes depend, in addition to the pore size, on the surface relaxivity (ρ) (Luo et al., 2015).

Surface relaxivity is a function of the pore wall composition,

* Corresponding author.
E-mail address: etelvino.novotny@embrapa.br (E. Henrique Novotny).

https://doi.org/10.1016/j.geoderma.2023.116363
Received 3 August 2022; Received in revised form 20 January 2023; Accepted 27 January 2023
Available online 9 February 2023

roughness, and clay and organic matter contents (Keating, 2014; Müller-Petke et al., 2015; Costabel et al., 2018; Keating et al., 2020). Consequently, this variable must be estimated by support methods (Costabel et al., 2018; Benavides et al., 2020), such as the relaxation time distribution calibrated to pore size (e.g., mercury intrusion porosimetry, 2D and 3D image analysis etc.) or to hydraulic properties such as water retention functions (Costabel and Yaramanci, 2013).

Additionally, the models consider the surface relaxivity uniform and homogeneous across all the different pore size classes (Schaumann et al., 2005; Benavides et al., 2020), or at most considering two surface relaxivity parameters, one for large pores and one for small pores (Jaeger et al., 2009; Meyer et al., 2018), which is a premise that is hardly met for natural porous materials (Liu et al., 2014; Benavides et al., 2017; Benavides et al., 2020).

According to Jaeger et al. (2009), the determination of the surface relaxivity is a tedious and time-consuming procedure, consequently, the use of relaxation mode to estimate the pore size distribution, and then the soil hydraulic properties, may have no time-saving advantage compared to the conventional methods used for the SWRC determination. To overcome this, Costabel and Yaramanci (2013) proposed the direct estimation of the SWRC from T_1 or T_2 measurements, avoiding the determination of pore size distribution, however, the method works satisfactorily only for samples with sand contents higher than 90 %. On the other hand, Müller-Petke et al. (2015) and Costabel et al. (2018) proposed a numerical method to access all relaxation and diffusion modes from T_1 and T_2 experiments when the spin system is outside the fast diffusion regime. Under such conditions, the ambiguity between pore size and relaxivity is resolved, but also this method does not apply to all systems, working only for those with a single and narrow pore size distribution. More recently, Costabel and Hiller (2021) proposed a complicated and time-consuming joint inversion method for NMR relaxation data that requires the NMR decays of the samples at saturation and at least one at partial saturation. Furthermore, the method strongly depends on the choice of the underlying capillary cross-section geometry, as well as requires the system to be in the fast diffusion regime. Like the previous methods, it only worked for sandy samples.

Seeking to overcome these limitations of NMR relaxometry, Song and collaborators (Song et al., 2000; Lisitza and Song, 2001; Song, 2003) proposed a new method to study porous materials. Named Decay due to Diffusion in Internal Field (DDIF), this method directly accesses the diffusion modes instead of the relaxation mode, using the field inhomogeneity (internal magnetic field gradient) produced by the natural susceptibility contrast in the sample. An elegant, clear and detailed explanation of this phenomenon, method and its application to determine the pore sizes of glass beads and natural rocks are presented in Song (2003). This method's physics and mathematical formulation can be found in Song (2003) and Liu et al. (2014). In addition, the validation of this method, using synthetic porous samples (glass beads and sintered solid glass microspheres) with known pore size distributions is given in de Pierri et al. (2022).

In this article, we propose the use of DDIF as a method to characterise the pore size distribution and to estimate the water retention curves of undisturbed soil samples. Because DDIF allow direct access to the NMR diffusion modes governed only by the pore size, and therefore, is independent of the unknown surface relaxivity, it can be used as an alternative and complementary method to the more standard NMR relaxometry techniques, mainly in samples with high internal magnetic susceptibility contrast.

2. NMR background: Description of the DDIF experiment

The interpretation of DDIF data involves the description of the magnetisation dynamics in terms of the so-called eigenmodes. The concept of eigenmodes is usually applied to describe physical systems with complex oscillatory behaviour. A general oscillatory system can be described in terms of a set of natural frequencies, so-called eigenfrequencies. The full system is then described as being comprised of a set of oscillatory components at the respective eigenfrequencies, the eigenmodes. Hence, an eigenmode is characterised by its frequency, amplitude (the number of oscillatory entities at the same eigenfrequency) and phase (the phase of the oscillations). The dynamics of the system can be characterised by a set of eigenmodes, i.e., by their frequencies, amplitudes and phases, which can be arranged in a matrix form. Thus, characterising a multicomponent oscillatory system in terms of its eigenmodes can be very advantageous since it allows to define what set of eigenfrequencies have a more significant contribution to their dynamics. This idea was explored in the NMR context by Song (2003), who shows that the eigenmode formalism, used in the original work of Brownstein and Tarr (1979), can describe very well the spin dynamics in experiments that selectively excite only a few eigenmodes. Additionally, the eigenmode frequencies are somewhat associated with the local NMR frequencies of the water inside the pores, so the set of eigenmode frequencies, amplitudes and phases that characterised the magnetisation dynamics could be associated with the pore distribution and pore geometry.

Based on Song (2003) and Liu et al. (2014) we explain briefly the method's principles as follows: the contrast of magnetic susceptibility between the solid and liquid phases of any porous material saturated with fluid when submitted to an external magnetic field, results in an internal magnetic field inhomogeneity (ΔB_z^i) in the pore space. Because the precession frequency is a linear function of the magnetic field, the position of the fluid molecules inside the pores is encoded in the NMR frequency of the corresponding magnetisation based on the local magnetic field they experience. After this initial "position labelling" the fluid molecules diffuses through the pore space, changing their position (and the B_z^i) and, consequently, their precession frequency. Once the total NMR magnetisation is comprised of the sum of the individual molecular magnetisation, the diffusion through the inhomogeneous magnetic field results in a decrease (decay) of the magnetisation profile. Furthermore, after some time, the diffusion of the molecules inside the pore space averages any non-uniformity in magnetisation, resulting in a spatially uniform magnetisation, and then, the further decay of this uniform magnetisation is governed only by the spin-lattice relaxation T_1 (referred as the ground mode of the spin-lattice relaxation). The DDIF experiment monitors the magnetisation intensity decay as a function of this diffusion time and, knowing the free self-diffusion constant (D) of the probing fluid, the pore size is determined (Song, 2003).

This is achieved by the NMR experiment represented in the pulse sequences scheme shown in Fig. 1. In the so-called sine pulse sequence (Fig. 1E), after the recycle delay d_1 (at least 5 T_1) the nuclear spins are in thermal equilibrium at the external magnetic field ($\mathbf{B_0}$), resulting in the thermal equilibrium magnetisation, initially in the direction of the external magnetic field ($\mathbf{B_0}$) (z-axis). This thermal equilibrium magnetisation is transferred to the transverse plane by the first $\pi/2$ radiofrequency pulse where it evolves in the transverse plane (x-y plane) during a short encoding time (t_e) (less than a full dephasing period – weak encoding regime), which provides the spatial labelling. Thus, at short encoding times, the dephasing is mainly due to the different precession frequencies of the nuclear spins that compose the macroscopic magnetisation caused by their distinct spatial positions at the non-uniform local magnetic field ΔB_z^i. After t_e, a second $\pi/2$ pulse is applied to store one magnetisation component in the direction of the external magnetic field, where it remains without further dephasing. After that, a variable diffusion time (t_{diff}) is introduced during which the magnetisation only experiences the effect of the spin-lattice relaxation (T_1). Finally, a third $\pi/2$ pulse brings the stored magnetisation component to the transverse plane where it evolves again in the inhomogeneous magnetic field during another encoding time t_e. Thus, the pulse sequence produces a stimulated echo at $2t_e + t_{diff}$, that is acquired. Because the formation of the stimulate echo depends on the magnetisation evolution (accumulated phase) during both encoding times, it reflects the correlation between spatial positions experienced by the

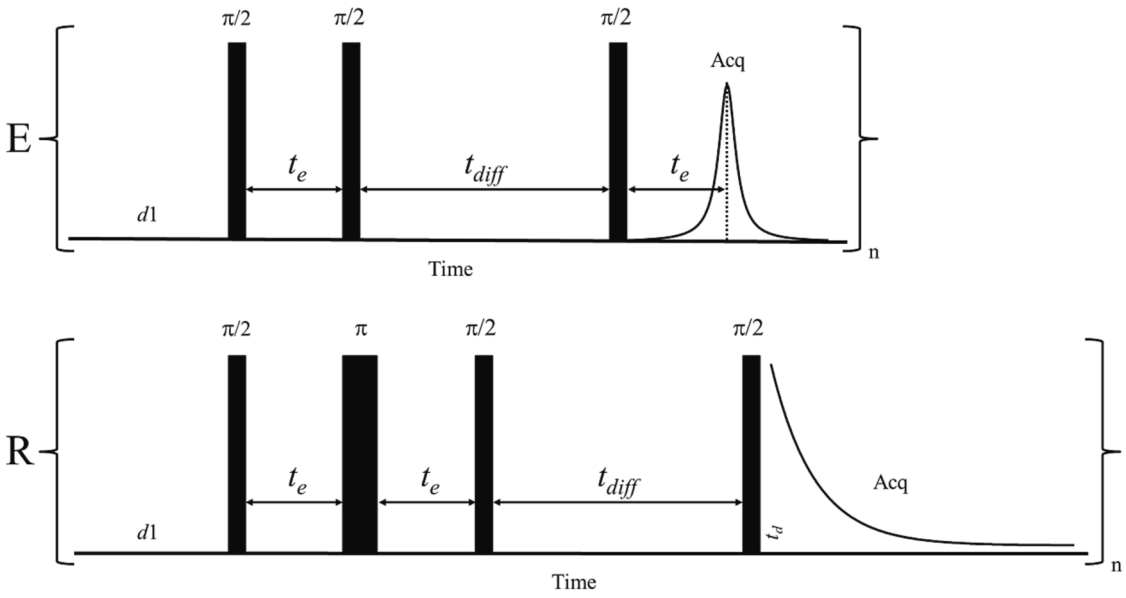

Fig. 1. Sine pulse sequence (E) and reference pulse sequence (R) used to detect the diffusion-only modes in porous media. Here $d1$ is the recycle delay (the time required for the system to reach the thermodynamic equilibrium, $\geq 5\ T_1$); $\pi/2$ and π are the 90° and 180° radiofrequency (rf) pulses, respectively; t_e is the encoding time and t_{diff} is the observation time of molecular diffusion. Acq is the signal acquisition (in fact, just a few points at the maximal stimulated echo and FID signals amplitudes are necessary), t_d is the dead time and n is the number of scans. The phase cycles are in Tab 1.

nuclear spins before and after t_e, which is dictated by the diffusion processes that occurred during t_{diff}. Therefore, the decay of the maximum amplitude of the acquired stimulated echo (E) depends on both the diffusion process (diffusion modes) and the spin-lattice relaxation (spin-lattice relaxation ground mode) during t_{diff}.

The effect of the spin-lattice relaxation ground mode on the echo amplitude can be subtracted by a decay that only depends on the spin-lattice relaxation ground mode. This is achieved by the pulse sequence shown in Fig. 1R. Named as reference pulse sequence, it is obtained by introducing a π pulse after t_e, which is followed by another encoding period t_e before storing the magnetisation for t_{diff}. This pulse scheme refocuses the magnetisation evolution at the $2t_e$, which makes the magnetisation stored during t_{diff} independent of ΔB_z^i (Song et al., 2000). Thus, the third $\pi/2$ pulse now generates a free induction decay (FID) (Levitt, 2001), whose initial amplitude acquired (R) only depends on the spin-lattice relaxation ground mode (Song, 2003). The resulting magnetisation decay is then used to correct the sine pulse sequence, keeping only the decay due to the diffusion in the internal magnetic field.

The normalised echo intensity arising from fluid molecules confined in a pore has an additional decay mechanism. If during t_{diff} they reach the pore wall, a corresponding contribution is encoded in the diffusion modes. Thus, knowing the velocity of the fluid molecules (the self-diffusion constant) and the time until reaching the wall (given by t_{diff}), it is possible to estimate the distance covered by the fluid molecules until they reach the pore wall, i.e., the pore size.

The pore size determined by relaxivity-dependent ground mode and the DDIF method considers the fast diffusion regime (Brownstein and Tarr, 1979; Song et al., 2000; Jaeger et al., 2009) defined by the constraint of the sink strength parameter (κ), calculated by Eq. (1), being $\ll 1$:

$$\kappa_{1,2} = 2\ r\ \rho_{1,2}\ D^{-1} \quad (1)$$

where 1 or 2 are the longitudinal or transversal relaxations (T_1 and T_2), respectively, and r is the pore radius.

The key point of the DDIF method is that the signal decay of diffusion modes is governed only by the pore geometry (size and shape), being independent of the unknown surface relaxivity (Song, 2003; Liu et al., 2014). In this paper, we used this method to determine the pore size distribution of undisturbed soil samples as well as to estimate the water retention curves from the pore size distribution. Table 1.

3. Material and methods

3.1. Soil samples

To validate this method, three soil belonging to the representative classes: Ferralsol, Arenosol and Luvisol, from the humid tropical climate zone, were chosen to obtain contrasting pore size distributions (Table 2).

Eight undisturbed samples of Ferralsol; seven of the Arenosol and four of Luvisol were analysed. The collection sites belong to a region of high geological heterogeneity, which allowed sampling of the three different soil orders within a distance of 50 km (Table 2). These soils represent 70 to 80 % of Brazilian soils.

The undisturbed samples were carefully collected by using Polyvinyl chloride (PVC) rings 4 cm high and 3.7 cm i.d. (43 cm^3). The sample diameter was conditioned to the size of the sample inlet of the NMR equipment model used (40 mm probe diameter), but it is close to the standard size used in conventional SWRC studies (5 cm i.d.). At each sampling site, disturbed samples were also collected to determine the particle size distribution of the studied soils (Table 2).

3.2. NMR measurements and data processing

All the ^{1}H NMR measurements were performed using the SpecFIT H50 benchtop NMR spectrometer (Fine Instrument Technology, São Carlos, Brazil) at a magnetic field of 0.35 T (^{1}H Larmor frequency of 15 MHz).

The undisturbed samples were saturated with deionised water for 24 h on a metal tray warmed in a water bath at a temperature of 31.5 °C, to optimise the required thermalisation of the samples with the internal temperature of the spectrometer (33.0 °C). For the NMR analysis, each sample was placed in a sealed polyethylene bag (ordinary plastic bag) to avoid water evaporation during the experiment. The plastic bags and PVC sample holders did not influence the analysis since there is no significant molecular diffusion in solids on the NMR timescale (Levitt, 2001). Additionally, the pulse sequences do not detect signals from solid polymers, since the ^{1}H–^{1}H dipolar coupling is not refocused (Levitt,

Table 1
Phase Cycling for the DDIF Sequences Liu et al. (2014).

Sine pulse sequence					Reference pulse sequence					
Step	ph1	ph2	ph3	Acq	Step	ph1	ph_π	ph2	ph3	Acq
1	90	0	0	90	1	0	90	0	0	0
2	270	0	0	270	2	180	90	0	0	270
3	90	180	0	270	3	0	90	180	0	270
4	270	180	0	90	4	180	90	180	0	90
					5	0	270	0	0	90
					6	180	270	0	0	270
					7	0	270	180	0	270
					8	180	270	180	0	90

ph1, ph2, and ph3 are the rf phases of the π/2 pulses in the order they appear in the pulse sequence; ph_π is the rf phase of the π pulse. Acq is the acquisition phase.

Table 2
Particle size distribution, texture, land use and localisation of the studied soils.

Soil order	Layer (cm)	Particle size (g kg^{-1})			Texture class	Land use	Coordinates	
WRB[1]		Sand	Silt	Clay			South	West
Arenosol	15	902	23	75	Sand	Fallow	22°34′96″	47°54′94″
Ferralsol	20	789	37	174	Sandy Loam	Annual Crops	22°43′61″	47°36′58″
Luvisol	25	570	254	176	Sandy Loam	Fallow	22°44′31″	47°31′31″

[1] WRB: World Reference Base (IUSS Working Group WRB, 2015).

2001). Despite this well-known fundamental basis, blank experiments, with empty holders and plastic bags, in the very same experimental conditions, were carried out. The results were, as expected, no signal.

The recycle delays were chosen to be five times longer than the ^1H spin-lattice relaxation time (T_1), as determined by the inversion-recovery (Levitt, 2001) experiments with recovery times from 0.1 to 10,000 ms. The spin-spin relaxation times (T_2) were measured using the Carr-Purcell-Meiboom-Gill (CPMG) pulse sequence (Levitt, 2001) with an inter-echo spacing time of 0.350 ms. The total water content filling the pore system at saturation was estimated by the conventional gravimetric method, i.e., by drying the water-saturated samples at 105 °C until constant weight, the weight difference between the fully-saturated and dried samples is the total water content.

The DDIF decay, free of spin-lattice ground mode contribution, (S, Eq. (2)) is obtained by subtracting the contribution of R in E, obtained by the pulse sequences described in the introduction and Fig. 1. The subtraction is made after scaling R by the ratio E/R at long t_{diff} (a_0), i.e., when both decays are parallel in the semilog plot, E decay becomes dominated only by the ground T_1 mode (Song, 2003; Liu et al., 2014):

$$S(t_{diff}) = E(t_{diff}) - a_0 R(t_{diff}) \quad (2)$$

As already mentioned, the DDIF experiment must be performed in the weak dephasing condition (weak encoding regime), i.e., the encoding time (t_e) must be shorter than the fastest dephasing ^1H due to the internal magnetic field inhomogeneities (T_i). This can be estimated by the difference $T_i^{-1} = T_{2,s}^{*\,-1} - T_{2,m}^{*\,-1} - T_{2,s}^{-1}$; where $T_{2,s}^*$ (s refers to

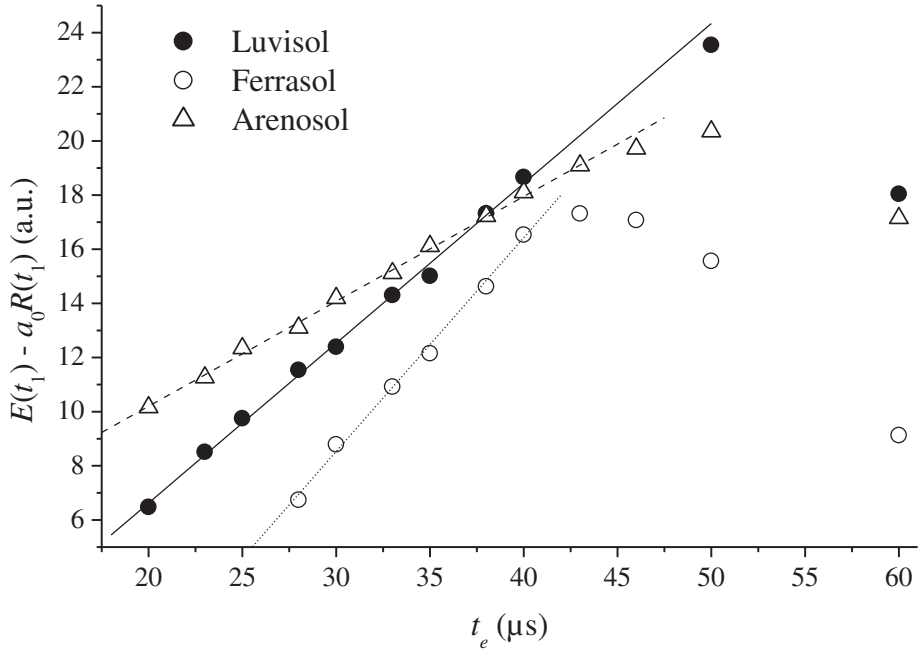

Fig. 2. Optimisation of the encoding time (t_e) for the studied soils. The signal amplitude, after removing the ground mode T_1 contribution by Eq. (2) (S), linearly increased up to $t_e = 40$ μs for all the studied samples. $E(t_1)$ and $R(t_1)$ are the initial amplitude of the E and R decays, respectively; a_0 is the scaling factor; and a.u. is arbitrary units.

sample) and $T^{*}_{2,m}$ (m for the magnet) are the effective transverse relaxation times (dephasing time), obtained from the decay of a single pulse Free Induction Decay (FID) (Levitt, 2001) of the water-saturated sample and of a water sample with the same geometry, respectively, and $T_{2,s}$ is the sample intrinsic transverse relaxation time obtained from a CPMG.

A more accurate optimised t_e is obtained from DDIF experiments carried out by varying t_e linearly from 20 to 60 μs in both pulse sequences (sine and reference, Fig. 1) for a single sample of each soil class, since the initial amplitude of the S decay (signal amplitude at the shortest t_{diff}) increases linearly with t_e at the limit of the weak encoding regime (Lisitza and Song, 2001). The results of the optimisation are shown in Fig. 2.

Finally, the two pulse sequences (Fig. 1) that measure the pore size distribution from DDIF (Song, 2003) were obtained with the adjusted t_e and 50 delays of the observation time of molecular diffusion (t_{diff}) logarithmically spaced from 10 μs to 5 s. For each t_{diff} step, 32 scans were performed and the d_1 was 1.5 s for all the samples, which resulted in a full analysis time (both pulse sequences) of about 1.5 h per sample.

After the NMR measurements, each sample was returned to the saturation tray before they were analysed by the SWRC conventional method (tension table and pressure plate extractor as will be described later).

The resulting multiexponential decays (S), inherent in this observed physical phenomenon (Brownstein and Tarr, 1979; Song, 2003; Ramos et al., 2009) were analysed using the Inverse Laplace Transform (ILT) with optimised Tikhonov regularisation (alpha) obtained by the L-curve (Hansen, 1992; Day, 2011). The ILT was performed using the approach Fast Laplace-like INverTer (Flint) proposed by Teal and Eccles (2015) and with the MatLab script available on https://github.com/paultnz/flint. To avoid overfitting, the alpha used was an order of magnitude higher than the optimised one (sub-optimised). It is important to stress that ILT is an ill-posed problem and the obtained distribution must be analysed carefully. The choice of alpha depends on the data quality (signal/noise ratio) and usually previous knowledge of the sample is used to find a more realistic solution (Whittall et al., 1991): i.e., how many exponential decay classes are expected. Since soils are complex systems, we believe that the found ILT solutions are realistic, and the pore classes found are based on the traditional classification of pore size distribution found in soils (Brewer, 1965). However, further studies, to determine the pore size distribution of the soil, must be carried out to confirm this.

The DDIF decay rate during t_{diff} ($1/\tau$), where τ is the time constant of the signal decay as a function of t_{diff}, depends on the geometry of the pores since it is controlled by the shortest pathway of the diffusion fluid inside the pore. This dependency is parametrised by ζ_1, the first positive root of the appropriate (geometry-dependent) transcendental function. For a pore with spherical geometry (spherical symmetry, shortest diffusion pathway in 3D) in which $a \approx b \approx c$, where a, b and c are the pore dimensions in the Cartesian x, y, z coordinates system, $\zeta_1 = 4.4934$; for a pore with a cylindrical geometry (elongated axial symmetry, shortest diffusion pathway in 2D) in which $a \approx b \ll c$, $\zeta_1 = 3.8317$; and for a pore with planar geometry (shortest diffusion pathway in 1D) in which $a \ll b$ and c, $\zeta_1 = \pi/2$ (Brownstein and Tarr, 1979; Grebenkov, 2008).

Therefore, the pore radii were obtained by rescaling the time decay τ by Eq. (3):

$$r = \zeta_1 \sqrt{D\tau} \tag{3}$$

where D is the molecular self-diffusion of the probing fluid (in the present case, water, $D = 2{,}651.9\ \mu m^2\ s^{-1}$). In this study, the scaling of the τ distributions was considering pores with cylindrical geometry.

3.3. Determination of the SWRC (conventional method)

To obtain the soil water retention curves, the undisturbed samples (the very same samples analysed by NMR) were saturated with deionised water and submitted to high matric potentials (−1, −2, −3, −6 and −10 kPa) using a tension table (Topp and Zebchuk, 1979) and low matric potentials using a pressure plate extractor (–33, –50, −100, −300 and −1500 kPa) (Klute, 1986). After finishing the drainage at each matric potential, the samples were weighed, the water content was determined by difference and the volumetric water content was calculated. The data were adjusted to the van Genuchten model (Eq. (4)):

$$\theta = \theta_r + \frac{\theta_s - \theta_r}{[1 + (\alpha|\Psi m|)^n]^{1-1/n}} \tag{4}$$

where θ is the volumetric water content ($m^3\ m^{-3}$), θ_s and θ_r, are, respectively the water content at saturation and residual saturation degree, and n and α are fitting parameters (van Genuchten, 1980).

3.4. Comparison between SWRC obtained by the conventional and NMR method

Since the SWRC obtained by the conventional method presents a very poor resolution, seeking to obtain comparable results with the conventional SWRC (Whittall et al., 1991), the ILTs of the S decays have been redone using very large regularisation parameters, which results in the desired loss of resolution, i.e., broadening of the distributions (Hansen, 1992; Day, 2011). Afterwards, the pore size scale was converted to the estimated soil matric potential, using the well-known Young-Laplace equation (Eq. (5)) by assuming the model of a bundle of cylindrical capillary tubes with a random distribution of radii (Kutilek and Nielsen, 1994; Stingaciu et al., 2010).

$$|\Psi_m| = \frac{20\,\sigma\cos(\alpha)}{g\,\rho_w\,r_{eq.}} \tag{5}$$

were Ψ_m is the soil matric potential ($|h|$, kPa), σ is the air-water surface tension ($\sigma = 0.07275\ N\ m^{-1}$), α is the contact angle between water meniscus and pore wall, g is the standard gravity ($g = 9.80665\ m^2\ s^{-1}$), ρ_w is the water density ($\rho_w = 1{,}000\ kg\ m^{-3}$) and $r_{eq.}$ the equivalent pore radius in m. Meniscus curvature was assumed 0° because the samples were considered fully wettable (Jaeger et al., 2009). The cumulative sum, from smallest to largest pore size, of the pore size distribution is proportional to the water content occupying the different pore size classes. After the conversion of the pore size scale to soil matric potential, using the Young-Laplace equation (Eq. (5)), the cumulative sum, scaled to the total water content at saturation, is the water content level at decreasing matric potential and was compared to the conventional SWRC.

It is important to point out some possible causes of divergences between pore radii and water retention estimated by this simple capillary tube model and natural soil samples (Tuller and Or, 2004) such as: i) the model considers that all pores with radiuses larger than $r_{eq.}$ are completely empty at a given Ψ_m and full of water in pores with smaller radii, which is unlikely true (Lourenco et al., 2012); ii) the occurrence of pores throats, tortuosity and imperfect pore connectivity diverge from the simple model of cylindrical capillary tubes (Kuncoro et al., 2014; Rabot et al., 2018); iii) furthermore, the $r_{eq.}$ is related to the local minimum of the pore (throat or bottleneck) radii, rather than to the average pore radius (Ghanbarian et al., 2016); iv) the difficulty to measure the contact angles between water menisci and pore walls (Lourenco et al., 2012); v) the shrinkage behaviour (not the case of the studied soils) that can change the soil volume during the desaturation process, resulting in changes of the water flow (Simms and Yanful, 2001; Sun and Cui, 2020).

3.5. General procedure used for determination of the soil pore size distribution and the soil water retention curve using DDIF experiments

For accurate and precise determination of the soil pore size distribution and the soil water retention curve the following procedure was

used:

1. Collect the undisturbed soil sample using a non-metallic sample holder such as PVC or Polyether ether ketone (PEEK) that fits into the NMR probe;
2. saturate the sample with water in the usual way, but using a water bath at the magnet temperature or thermalise the samples before the measurements, weigh the water-saturated sample;
3. determine the spin–lattice relaxation time (T_1) of the saturating water using the conventional Inversion-Recovery pulse sequence;

Comment: This is an important NMR parameter to determine the recycle delay (d1 $\geq 5\ T_1$), which is the time that needs to be waited for the sequence to be repeated and accumulate scans. Alternatively, the T_1 of the water used to saturate the sample can be used. The ubiquitous paramagnetic ions (e.g., Fe^{3+}; Mn^{2+}; Cu^{2+} etc) of the soil solution will shorten the T_1 of the saturating water (T_{1b} in the equation below), furthermore the contribution of the wall of the pores will decrease T_1 as well (the second right term in the equation):

$$\frac{1}{T_1} = \frac{1}{T_{1b}} + \rho_1 \frac{S}{V}$$

where S/V is the surface-to-volume ratio of the pore.

4. determine the encoding time (t_e) based on the internal magnetic field inhomogeneity;

Comment: a first estimate can be obtained by determining the relaxation rate due to the internal magnetic field inhomogeneities (T_i^{-1}). t_e must be shorter than T_i, which is given by:

$$\frac{1}{T_i} = \frac{1}{T_{2,s}^*} - \frac{1}{T_{2,m}^*} - \frac{1}{T_{2,s}}$$

where $T_{2,s}^*$ (s for the sample) and $T_{2,m}^*$ (m for the magnet) are the effective transverse relaxation times (dephasing time), obtained from the exponential decay fitting of a Free Induction Decay (FID) signal of the water-saturated sample and a sample of water with the same geometry, respectively, and $T_{2,s}$ is the sample intrinsic transverse relaxation time obtained from an ordinary CPMG experiment. Usually the contribution of $T_{2,s}$ is negligible due to its long value and the CPMG experiment can be dispensed. Furthermore, $T_{2,m}^*$ tends to be constant and must be checked only eventually.

After this first estimative, perform the E and R experiment with the shortest (E_s and R_s) and longest (E_L and R_L) t_{diff} (e.g., 2 s) by varying linearly t_e around this first t_e estimative. Plot E_s-E_L/R_LR_s from the obtained signals amplitude against t_e and select the maximal t_e in the linear region of the plot. This full calibration just took 15 min using our equipment.

5. perform the full E and R experiments using the pre-defined d1 and t_e with 50 logarithmically spaced t_{diff} and a suitable number of scans (appropriate signal/noise ratio);
6. obtain the soil water content at a known matric potential in a conventional pressure plate, avoiding the asymptotic extreme of the water retention curve, being around the inflexion the best (e.g., -Ψ of 60 or 100 cm);
7. obtain the total water content at saturation by drying the samples at 105 ºC until constant weight, the weight difference between the fully saturated and dried sample is the total water content;
8. normalise the amplitudes (A_n) and plot semilog A_n versus t_{diff} and define the t_{diff} when the E decay turns dominated by T_1 (the E and R decays are parallel), calculate a_0 to correct the R intensity. We got better results using the average of several t_{diff} after the decays present the same slope because at the longest t_{diff} both signals are close to full relaxation and so close to 0 with a relevant noise;
9. subtract the contribution of R in E by Eq. (2), rescale S by the total water content obtained in 7;
10. perform the Laplace Inversion of S with appropriate Tikhonov regularisation (L-curve) to obtain the decay time τ distribution;
11. rescale τ to obtain the pore size by Eq. (3). This is the sample pore size distribution;
12. recalculate the Laplace Inversion of S with an oversized Tikhonov regularisation seeking to obtain a smoother water retention curve, similar to the conventional SWRC, sum cumulatively the obtained distribution from smallest to largest pore, rescale the pore size axis to matric potential by Eq. (5) (bundle of cylindrical capillary tubes model) or by the preferred alternative model;
13. recalibrate the matric potential axis by the value obtained in 6 (e.g., -Ψ of 60 or 100 cm), by finding, in the above integrated distribution, the closest water content value obtained in 6. The ratio between both matric potentials, the experimental from pressure plate (60 or 100 cm) and the estimated by the Young-Laplace equation (Eq. (5)), or by the alternative model chosen, is the calibration factor. This final calibration step is merely fine tuning and, from a physical standpoint, is not as necessary as in common empirical approaches (e.g., Costabel and Yaramanci, 2013). This is done only to get an optimum coincidence with the conventional SWRC measurements in order to overcome systematic discrepancies between model and reality, as will be described and discussed later.

4. Results and discussion

4.1. Optimisation of DDIF experiments for soil samples

DDIF experiments require a proper choice of the evolution times t_e, which is a function of the magnetic susceptibility of the sample. A representative example of this optimisation is shown in Fig. 2.

Analysing the three soil classes, an optimised common t_e of 40 μs was found and used. This value is shorter than the one used in glass beads and porous rocks (Lisitza and Song, 2001; Song, 2003; Liu et al., 2014), confirming the strong internal magnetic field gradient for these samples rich in paramagnetic impurities, this has additional practical interest since the small pore size limit is given by $r\ \sqrt{Dt_e}$ (Song, 2003), and then, with shorter t_e, smaller pores can be detected. The soil with the highest magnetic susceptibility (Ferralsol) presented the shortest optimised t_e (40 μs). The common t_e of 40 μs was chosen for all soils because there is only a small signal loss for soils with sub-optimal t_e, but using it, we standardise the analyses and also the lowest limit of pore size detected.

The spin dephasing rate is a function of the internal magnetic field gradient. Because of this, the optimised t_e is inversely proportional to the intensity of the internal magnetic field gradient and to the magnetic susceptibility contrast. Because of this, for DDIF purposes, the proper calibration of t_e dispenses with knowledge of the sample magnetic susceptibility. In this sense, in our opinion, the easy calibration of t_e to provide a direct indication of the applicability of the method, without the need for additional analyses, is an advantage of the proposed protocol.

On the other hand, the large pore size limit is a function of T_1: $r = \zeta_1\sqrt{DT_1}$ (Song, 2003). Since water bulk T_1 depends on the soil water composition (i.e., the presence of paramagnetic ions), the upper limit is also sample dependent. For the studied samples, considering pores with a cylindrical shape, the observational limits are from ~0.26 to ~273 μm, in the range of ultramicropore to fine macropores (Brewer, 1965) that represent the most relevant pore sizes related to soil water retention and water supply for the plants.

An alternative to increasing the upper limit would be to increase the measurement temperature. This is possible because T_1, at the used magnetic field (Levitt, 2001), and D (Holz et al., 2000) increase with temperature. Based on these Physical properties, increasing the

measurement temperature up to 80 ºC the upper limit could be increased by a factor of almost three (up to ~900 μm). However, the full measurement time would also triple, since the recycle delay (d1 ≥ 5 T_1) also needs to be increased. There are other alternatives to increase T_1, and hence the upper limit of the pore size that can be detected, such as degassing the water used to saturate the samples, removing paramagnetic ions from the soil solution or even using a mixture of H_2O/D_2O (Tadimalla and Momot, 2014).

4.2. Using DDIF experiments to obtain the pore size distribution of soils.

Fig. 3 shows typical raw data (raw decay curves from *E* and *R* experiments) as well the decay free of spin-lattice relaxation (*S* decay obtained from Eq. (2)).

Fig. 4 presents examples of typical pore size distributions, after ILT of the *S* decays, using sub-optimised Tikhonov regularisation obtained by the L-curve. The scaling of the τ distributions was considering pores with cylindrical geometry. However, since all the samples were in the intermediary or even slow diffusion regime (see below), the obtained pore size could be underestimated since the higher eigenmodes might shorten τ (Brownstein and Tarr, 1979). Decays can even be misadjusted by ILT as small pores if the alpha is small enough. These are the "ghost pores" mentioned by Costabel and Hiller (2021) and will be discussed in detail below.

It is worth mentioning that, the L-curve test provides an optimised regularisation parameter that best fits the experimental decay and should reflect the pore size distribution. However, further studies, using, for example, ultrahigh-resolution tomography are needed to confirm to what extent the ILT with the sub–optimal regularisation parameter alpha is close to the "true" pore distribution.

4.3. Using DDIF experiments to obtain SWRC in soils.

Based on the capillary-tube bundle theory (Jury and Horton, 2004), matric suction is related to an equivalent porous radius by the Young-Laplace equation (Eq. (5)) (Stingaciu et al., 2010), and thus, the integration of the pore size distribution, after converting the pore sizes to Ψ_m, using the capillary model, could estimate the SWRC. However, to translate the pore size function into the SWRC is not a direct task, not only due to the poor resolution of the conventional SWRC, but also due to the water dynamics in the soil, which is not a discrete (with steps) phenomenon, but continuous. For example, usually, a unimodal van Genuchten empirical function is used to represent the SWRC data, i.e., it is supposed that the soil has a unimodal pore size distribution regarding hydraulic properties. At the best, a bi-modal distribution is expected (Dettmann et al., 2014).

Although the possibility of obtaining SWRC from a more realistic pore sizes distribution is an important advantage of using NMR methods in general, the well-resolved pore size distribution obtained by DDIF with sub-optimal regularisation parameter leads to more featured SWRC prediction than the conventional analysis. This is demonstrated in Fig. 5a and Fig. S1 (Supplementary material), where the SWRCs obtained from DDIF using sub-optimal alpha (the integral of the pore size distribution) clearly show a pattern with steps which is not observed in SWRC using the conventional method. Thus, to provide more comparable results between the SWRC obtained by DDIF and the conventional method, the ILT was recalculated using an oversized (larger alpha compared with the sub-optimal value) Tikhonov regularisation.

As observed in Fig. S2, larger alpha smooths the estimated decay without changing its general shape. The obtained χ^2 values of the ILT fits, or even a simple visual analysis, clearly show that the ILT fitting curves with sub-optimal or oversized alpha are mostly equivalent. It is also worth mentioning that the gain using sub-optimised alpha concerning the fitting of the DDIF decay is minimal, which makes the pore size distribution obtained with the oversized alpha an acceptable mathematical solution. In addition, fitting the van Genuchten to the NMR-based SWRC with optimal or oversized alpha results in similar values (data not showed) since it fits the average curve (non-linear least squares).

Furthermore, the optimised alpha fits better the decay, but this contains "undesirable" real information, i.e., the contribution of the higher eigenmodes (n >1), especially outside the fast diffusion regime (see below). Therefore, for the practical issue: use the optimised alpha, if a step-wise result is desired. Otherwise, if a smooth SWRC is preferable, increase alpha until you obtain it. According to Whittall et al. (1991): "Our philosophy is to construct a variety of minimum structure solutions which are likely to have the essential features required by the data and be consistent with physical reality." If the target physical reality is the pore size distribution: use the optimised alpha (even increasing the number of scans, seeking to better S/N ratio, and increasing the number of t_{diff}), on the other hand, if the target is the SWRC, smooth the curve.

The general shape of the SWRC estimated directly from the pore size

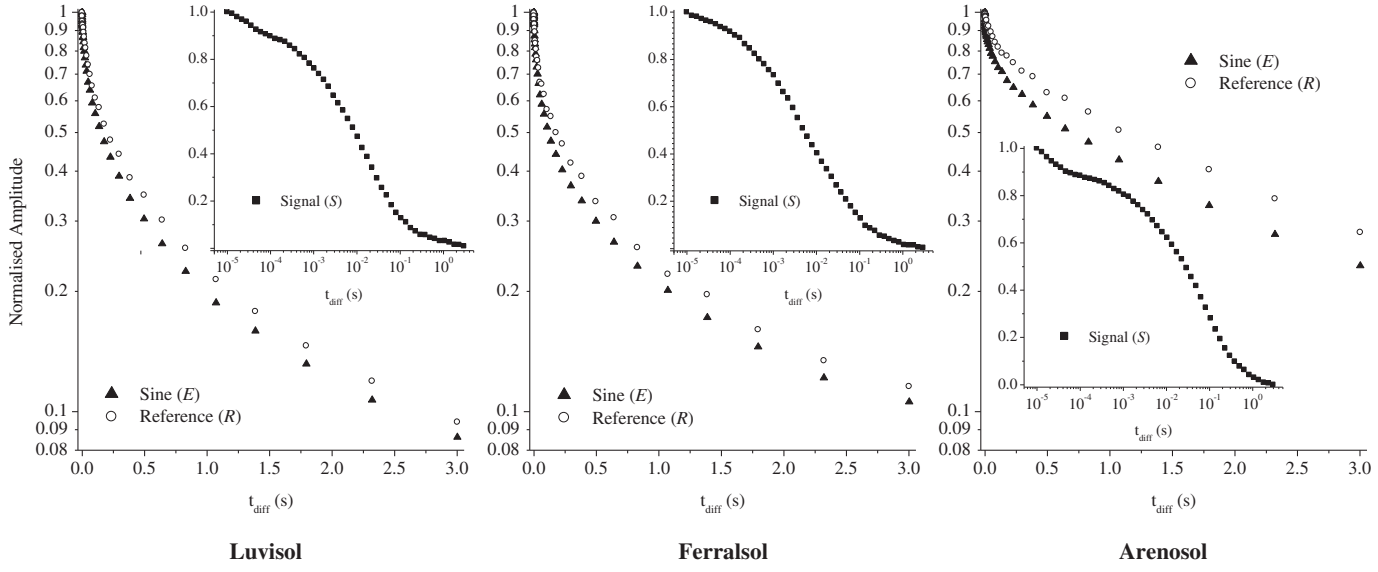

Fig. 3. Typical normalised experimental raw data from *E* (circles) and *R* (triangles) experiments. The inset gives the result of *S* (squares) from Eq. (2), the decay used to estimate the pore size distribution.

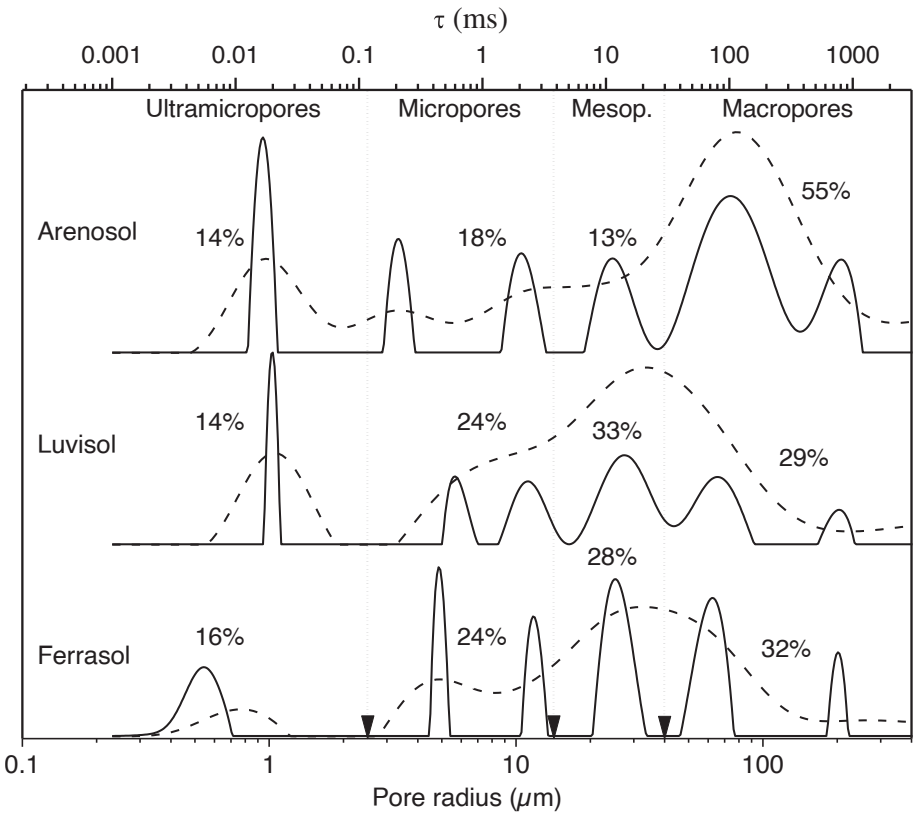

Fig. 4. Pore size distribution obtained from DDIF considering cylindrical pores. The solid lines are the distribution with sub-optimised Tikhonov regularisation and the dashed lines are the distribution with an oversized Tikhonov regularisation used to estimate the SWRC. The percentages are the contribution of each pore size class to the total porosity (area under the sub-optimised distributions). The pore size class indicated in the top x-axis is based on Brewer (1964).

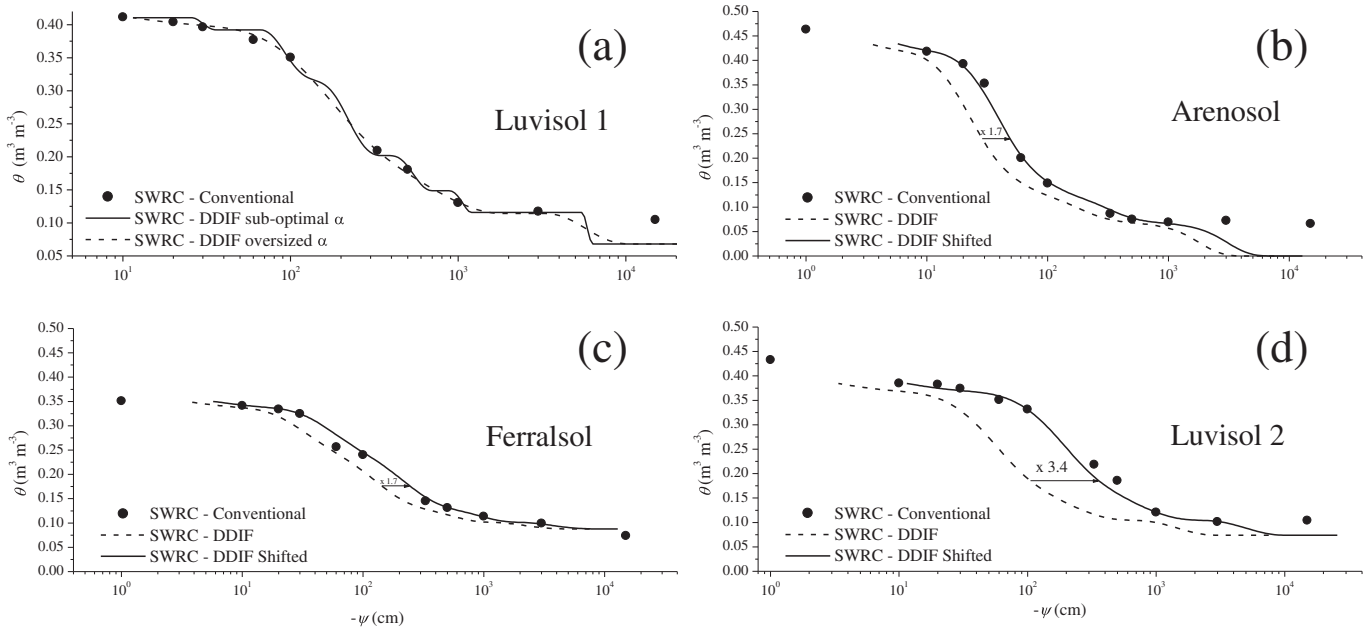

Fig. 5. Typical SWRC estimated from pore size distribution obtained from DDIF experiment (lines) compared to SWRC obtained by the conventional method using tension table and pressure plate extractor (black bullets). (a): The solid line is the SWRC obtained from the DDIF method with a sub-optimal Tikhonov regularisation while the dashed one is with the oversized Tikhonov regularisation. (b-d): The dashed line is the SWRC obtained directly from the pore size distribution from the DDIF method while the solid one is the same curve after shifting the Ψ_m scale by a factor of 1.7 (Arenosol and Ferralsol) or 3.4 (Luvisol). These factors were obtained after calibration against the Ψ_m of the reference method at −100 cm (Costabel and Yaramanci, 2013). The same graphs for all the analysed samples can be found in the Supplementary material (Fig. S3).

distribution obtained from the DDIF experiment with oversized regularisation parameter is similar to the SWRC obtained by the conventional tension table and pressure plate extractor methods (Fig. 5 and Fig. S3).

Although, the energy of the water retention (the Ψ_m) was systematically underestimated. Costabel and Yaramanci (2013) proposed, with success, a shift of the relaxation time distribution using only one pressure plate measurement at 63 cm, however, as discussed in the introduction, they were able to estimate the SWRC only for samples with more than 90 % of sand. They stressed that this shift only changed the α parameter in the van Genuchten model, maintaining the n parameter constant, essential to predict the relative hydraulic conductivity.

The same procedure can be used for the pore size distribution obtained by DDIF to estimate the SWRC. For the studied soils, using $\Psi_m = -100$ cm to calibrate the estimated Ψ_m from NMR-based SWRC, this shift was 1.7 for Arenosol and Ferralsol and 3.4 for Luvisol (Fig. 5 and Fig. S3).

This systematic disagreement between the conventional SWRC and the one estimated from porosity data occurs because the soil is not an ideal capillary-tube bundle system and predictive models for SWRC from porosity data, or the inverse problem, fail (Hunt and Ewing, 2009). It is important to stress that the equivalent pore radius ($r_{eq.}$) in Eq. (5) is not the effective (geometrical) pore length (Kutilek and Nielsen, 1994) as well as the $r_{eq.}$ is related to the local minimum of the pore (throat) radii, rather than to the average pore radius (Ghanbarian et al., 2016). To correct this difference, a factor to adjust pore shape, connectivity, throats and tortuosity is necessary, whatever the method of porosity determination (Bittelli and Flury, 2009; Stingaciu et al., 2010; Chen et al., 2017; Costabel and Hiller, 2021). This shift can be necessary also due to the imprecise premiss of considering soil pores as cylindrical pores, since ζ_1 is 4.4934 for spherical; 3.8317 for cylindrical and $\pi/2$ for planar geometries, and so, the pore size can be overestimated, and Ψ_m underestimated in the same proportion (Eq. (5)), if the real pore shape is not cylindrical. This underestimation of Ψ_m can be down to a factor of $3.8317/(\pi/2) = 2.4393$.

For Luvisol and, especially, for Arenosol, the lowest Ψ_m of the conventional SWRC (–15,000 cm for Luvisol and −3,000 and −15,000 cm for Arenosol) present higher water contents than the SWRC estimated from the pore size distribution obtained from the DDIF experiment, resulting in a dry-end curvature deviation (Hunt and Ewing, 2009). This can be due to the well-known failure of the pressure plate to continuously drain the soil at low water potentials. Under these conditions, the

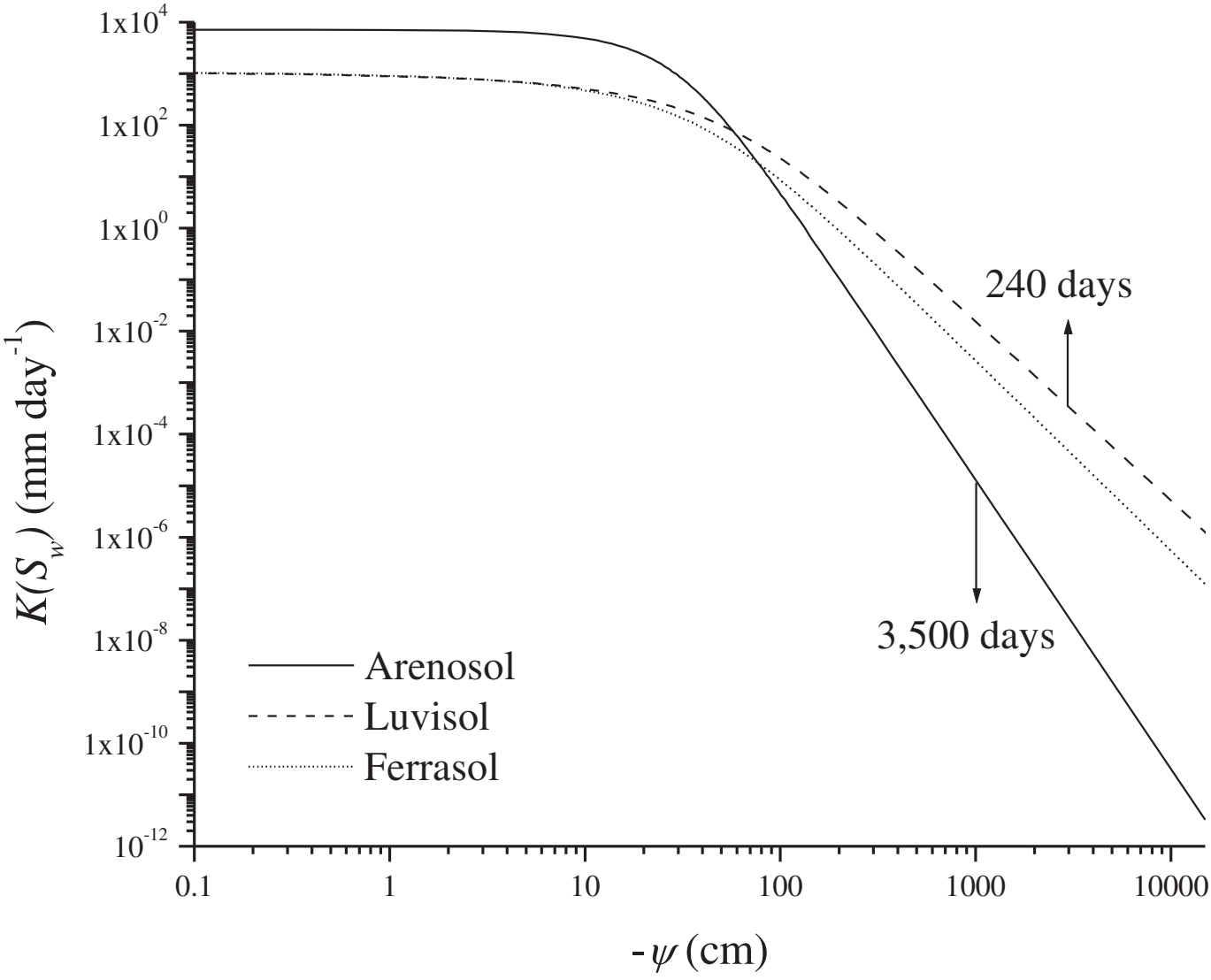

Fig. 6. Predicted hydraulic conductivity curves versus pressure head (Ψ) using the Mualem model and van Genuchten parameters obtained by fitting the conventional SWRC data with Eq. (4) for Arenosol, Luvisol and Ferralsol showed in Fig. 5. The arrows indicate the time necessary for a reduction of 1 % in the water saturation at the corresponding Ψ, using $\frac{dS_w}{dt} = \frac{K(S_w)}{z\phi^2}$ (Ghanbarian and Hunt, 2017).

samples never reach equilibrium due to the poor contact between the sample and the porous plate (Campbell, 1988; Stingaciu et al., 2010). This process is more critical for sandy soils (Campbell, 1988) and may explain the divergence observed for the sandy soil in this study.

Ghanbarian and Hunt (2017) demonstrated that low conductivity at the dry end of the SWRC results in a non-equilibrium condition during practical experimental time. Estimating the hydraulic conductivity of the studied soils using the Mualem model and the van Genuchten parameters obtained by Eq. (4) (Fig. 6), it is possible to calculate a rough approximation of the time necessary for the samples to reach the equilibrium using Equation (5) given in Ghanbarian and Hunt (2017):

$\frac{dS_w}{dt} = \frac{K(S_w)}{z\phi^2}$; where S_w is the water saturation, $K(S_w)$ the unsaturated hydraulic conductivity, z the sample height and ϕ the porosity. For the studied samples, with a height of 4 cm, a reduction of 1 % of the water saturation would take, for the Arenosol at a Ψ_m = -1,000 cm (after which the dry-end disagreement begins – Fig. 5), at least 3,500 days, while for the Luvisol (Ψ_m = -3,000 cm) at least 240 days, much longer than the experimental time used. That is most probably the main reason for the observed dry-end disagreement.

Furthermore, the NMR-based SWRC for Ferralsol and Luvisol samples did not reach the zero line, even at the highest matric potential (Fig. 5 and Fig. S3) because, to avoid overfitting due to extrapolation, the ILT was calculated in the same range of the experimental t_{diff} interval, i.e., from 10 μs to 5 s, and then, with the oversized Tikhonov regularisation, the left side (the smallest pore size limit) of the ultramicropores distribution sometimes was truncated, not starting at zero, which resulted in an integrated pore size distribution that did not reach zero at the lowest Ψ_m. From the SWRC point of view, this makes sense since water in the ultramicropores (essentially residual water in the van Genuchten model) is not drained at this Ψ_m and this water is unavailable for the plants, i.e., at the permanent wilting point ($\Psi_m < -15{,}000$ cm).

Future research, using alternative methods more accurate to determine the water saturation at the dry range (e.g., dewpoint potentiometer), may confirm these hypotheses.

In the case of Ferralsol, the slight disagreement between the proposed method and the conventional SWRC at the lowest matrix potential (-15,000 cm) can be explained by the fact that the clay content (17.4 %) favours the presence of microaggregates, typical of Ferralsols, whose inter-microaggregate porosity may be below 0,1 μm (Bartoli et al., 1992) and therefore out of the lowest detection limit of DDIF. This hypothesis may be confirmed in the future by microtomographic images. The lowest detection limit can be lowered using shorter encoding time (t_e) since $r\sqrt{Dt_e}$, however penalising the signal-to-noise ratio (Fig. 2), which may require more scans and consequently more analysis time.

4.4. Further information provided by DDIF experiments in soil samples.

With the pore size distribution, the estimation of the SWRC and subsequent interpretations, for example, to estimate the unsaturated hydraulic conductivity, the choice between the various models mentioned by Ghanbarian and Hunt (2017): a bundle of straight capillary tubes; bundle of tortuous capillary tubes; critical path analysis; effective-medium approximations; percolation theory; pore network models or lattice-Boltzmann methods, is at the discretion of the researcher and is beyond the scope of this work. And even our choice of model to estimate the SWRC, that is, a bundle of straight capillary tubes, which is simple, well-known and widely applied in soil physics is arbitrary, but it provided very similar results to the conventional SWRC, therefore following the criterion Occam's razor, we believe to be sufficient for the paper's proposal.

Since the reference experiment decay with T_1 (Song, 2003), it is possible to obtain this important parameter from the DDIF method (Fig. 7). However, the T_1 obtained from the reference experiment is systematically shorter (15 %) than the one obtained by the standard Inversion-Recovery experiment, but is still a good estimative of T_1.

The logarithmic means of T_1 and of the pore radius (r) of each peak from their respective distributions were calculated. With these estimated pore radii (r) and their correspondent T_1, i.e., pairs r and T_1 determined graphically by plotting both distributions together, it is possible to calculate the longitudinal surface relaxivity ρ_1 by $\rho_1 = r/nT_1$, with n = 1, 2 or 3 for planar, cylindrical, or spherical geometries (Fig. 8 for 2D geometry).

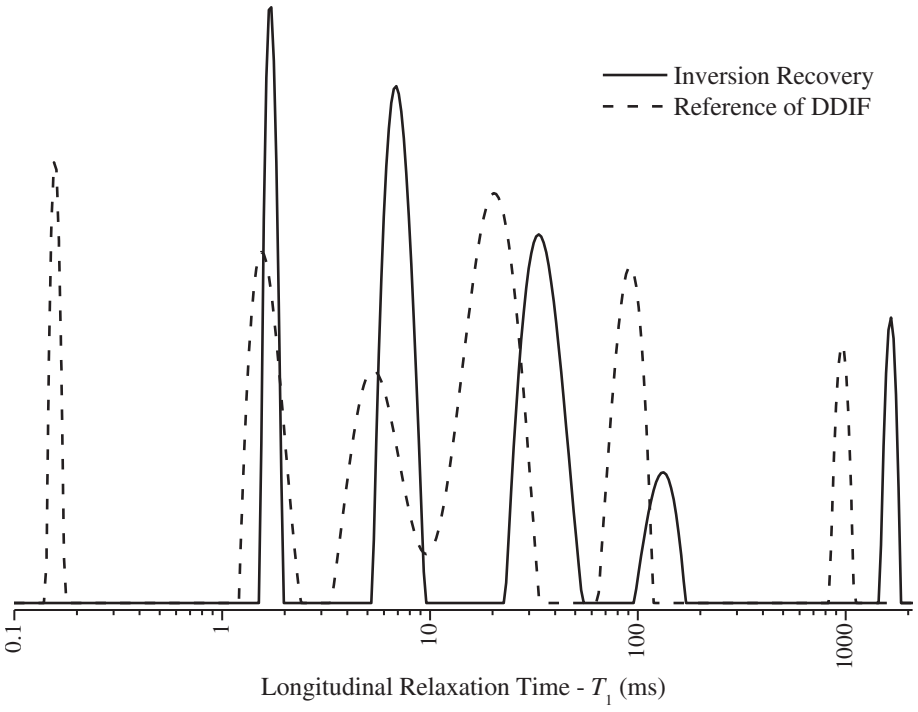

Fig. 7. Longitudinal relaxation (T_1) distribution for Luvisol obtained from the reference experiment of the DDIF (R) method and by the conventional Inversion-Recovery experiment.

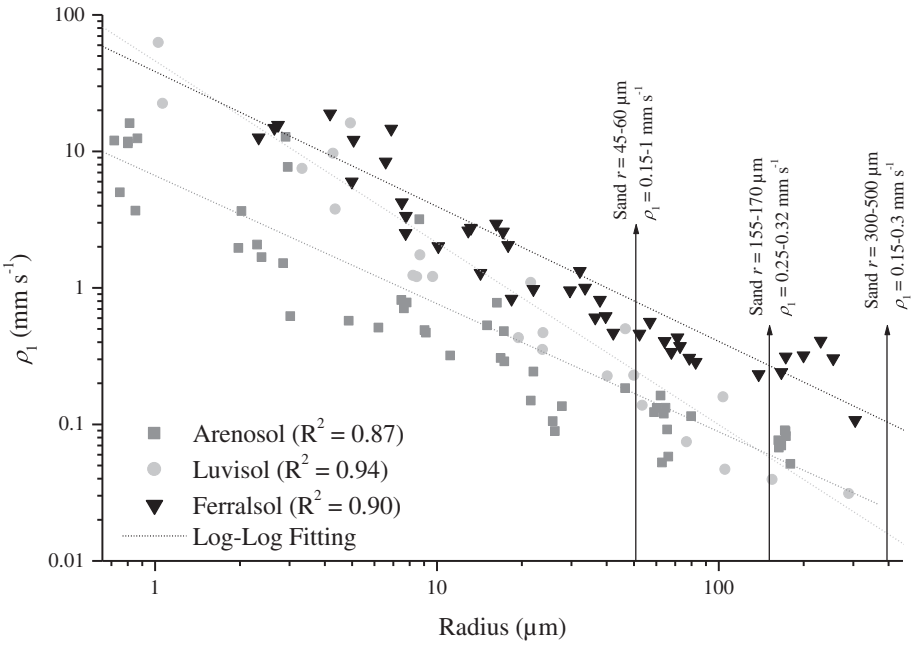

Fig. 8. Spin-lattice surface relaxivity (ρ_1) of the studied soils. The arrows indicate typical values obtained from sand samples with similar pore sizes (Müller-Petke et al., 2015).

The estimated ρ_1 for the macropores (indicated by the arrows in Fig. 8) are in good agreement with the ones reported by Müller-Petke et al. (2015). However, it is clear that ρ_1 linearly decreases, on a log–log scale, with the increase in pore size, corroborating with Liu et al. (2014) and Benavides et al. (2017), Benavides et al. (2020). Since T_2 is $\leq T_1$, the ρ_2 is still larger than ρ_1 and also decreases linearly, in the log–log scale, with the pore length scale (data not shown).

This nonuniform ρ throughout the different pore size domains imposes more limitations to the usual proposal that estimates the pore size distribution using the conventional (ground mode) relaxation (T_1 or T_2) data, even using two surface relaxivity parameters, one for large pores and one for small pores, as discussed by Jaeger et al. (2009). This strong dependency of ρ with pore size, especially with the smaller pores, could explain why Costabel and Yaramanci failed to estimate the water retention curves from the relaxation data (T_1 and T_2) in samples with less than 90 % of sand (Costabel and Yaramanci, 2013).

The orthogonal and spatial characteristics of the eigenmodes classify them into two categories: the ground mode is the relaxation mode, while all the highest modes are diffusion-only modes (Song, 2003). The proposed method, since it is based only on the diffusion modes without any contribution of the ground mode, is independent of ρ and then prescinds any additional information or premises. Furthermore, after the correction by the reference pulse sequence, the DDIF method is also insensitive to the bulk relaxation, another issue accordingly Müller-Petke et al. (2015) for the methods proposed by Müller-Petke et al. (2015); Costabel et al. (2018) and Yu et al. (2019).

Concerning the diffusion regime, calculating κ_1 (Eq. (1)) we found that all the samples are in the intermediate or even slow diffusion regimes. For these cases, the higher eigenmodes start to contribute significantly to the signal intensity and consequently to its decay (Fig. S4), resulting in, for the same pore size, the observation of shorter decays due to the contribution of the highest modes (Brownstein and Tarr, 1979), thus the pore size will be underestimated.

With the oversized Tikhonov regularisation factor used, the highest eigenmodes are merged with the first one. Thus, considering until the sixth eigenmode (less than 4 % of the total intensity), the error in the average pore size will be less than 30 %, even in the slow diffusion regime for any geometry (Fig. 9).

However, this contribution of higher eigenmodes to the overall decay, for being outside of the fast diffusion regime, can result in artefacts if direct scaling of τ to pore size is made, i.e., "ghost" pores (Costabel and Hiller, 2021). This happens because the diffusion cannot even out (average) the magnetisation decay through the whole space of each pore within the time scale of the experiment and, even in a system with a single pore size distribution, the relaxation decay will be multi-exponential (Brownstein and Tarr, 1979; Keating and Knight, 2010; Keating, 2014). Since the presence of small pores (micropores and smaller) in the Arenosol is low, this artefact is probable and could be verified through ultrahigh-resolution tomography of the samples, for example. However, this is out of the scope of this paper. Additionally, the shift of the matric potential in the SWRC estimated by ILT, using the

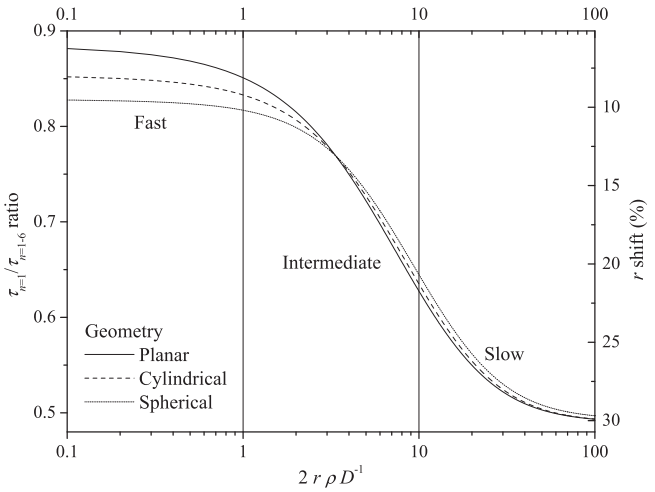

Fig. 9. Ratio of the first-mode decay time (n = 1) to the overall highest eigenmodes (n from 1st up to 6th) decay times ($\tau_{n=1}/\tau_{n=1\text{-}6}$) as a function of the sink strength parameter $\kappa = 2\ r\ \rho\ D^{-1}$ and resulting shift (error) in the pore radius (r) estimated by ILT considering only the first eigenmode. The ILT used an oversized Tikhonov regularisation factor of the simulated decays. Three geometries (planar, cylindrical, and spherical) are considered. Based on Fig. 1 by Brownstein and Tarr (1979).

oversized Tikhonov regularisation factor, also takes into account this potential systematic error in the pore size, confirmed by the good similarity between the estimated and conventionally determined SWRCs (Fig. 5 and Fig. S3). Furthermore, another way of comparing the results obtained by the proposed method with the reference is fitting the empirical van Genuchten equation (Eq. (4)). The parameters α and n, estimated from both methods, were equal in the fitting error range (Fig. 10) and confirm the potential of the proposed method.

5. Remarks on the advantages and possible limitations of using the DDIF method in soil samples.

The proposed method is fast (1.5 h per sample compared with weeks to months by the conventional method), accurate and precise to determine the soil pore size distribution and the SWRC (Fig. 5 and Fig. S3).

The selected soils, besides being representative of Brazil, corresponding to more than 70 % of Brazilian soils (Santos et al., 2018), pushed the limits of the DDIF method toward complex, unconsolidated and with very large magnetic susceptibility, indicated by the very short t_e (40 μs), compared with the usual ms range fitted for porous rocks and glass beads (Lisitza and Song, 2001; Song, 2003; Liu et al., 2014). Unlike recent proposals in the literature (Müller-Petke et al., 2015; Costabel et al., 2018; Yu et al., 2019), which, in addition to the ground mode, try to access the higher eigenmodes (first and second) by numerical methods under very restricted constraints, i.e., samples with a narrow pore size distribution, uniform ρ, and outside the fast diffusion regime, the DDIF approach used here accesses only the higher modes experimentally without constrains about the pore size distribution and/or surface relaxivity (ρ).

Furthermore, in contrast to the above-mentioned methods, the proposed one is based only on the diffusion modes, whose decays times are closer to each other than to the ground mode (see Fig. 1 in Brownstein and Tarr, 1979 and Fig. S5). Then, in addition to being independent of ρ, they are also affected by κ (the diffusion regime), but in much lesser extension than the ground mode (Fig. S5). This fact results in a maximal error of 30 % in the pore size estimation (Fig. 9) due to a misassumption about the diffusion regime. Besides that, since the DDIF method has a correction for T_1 decay, it is independent of the bulk relaxation, another issue accordingly Müller-Petke et al. (2015) for the methods proposed by Müller-Petke et al. (2015); Costabel et al. (2018) and Yu et al. (2019).

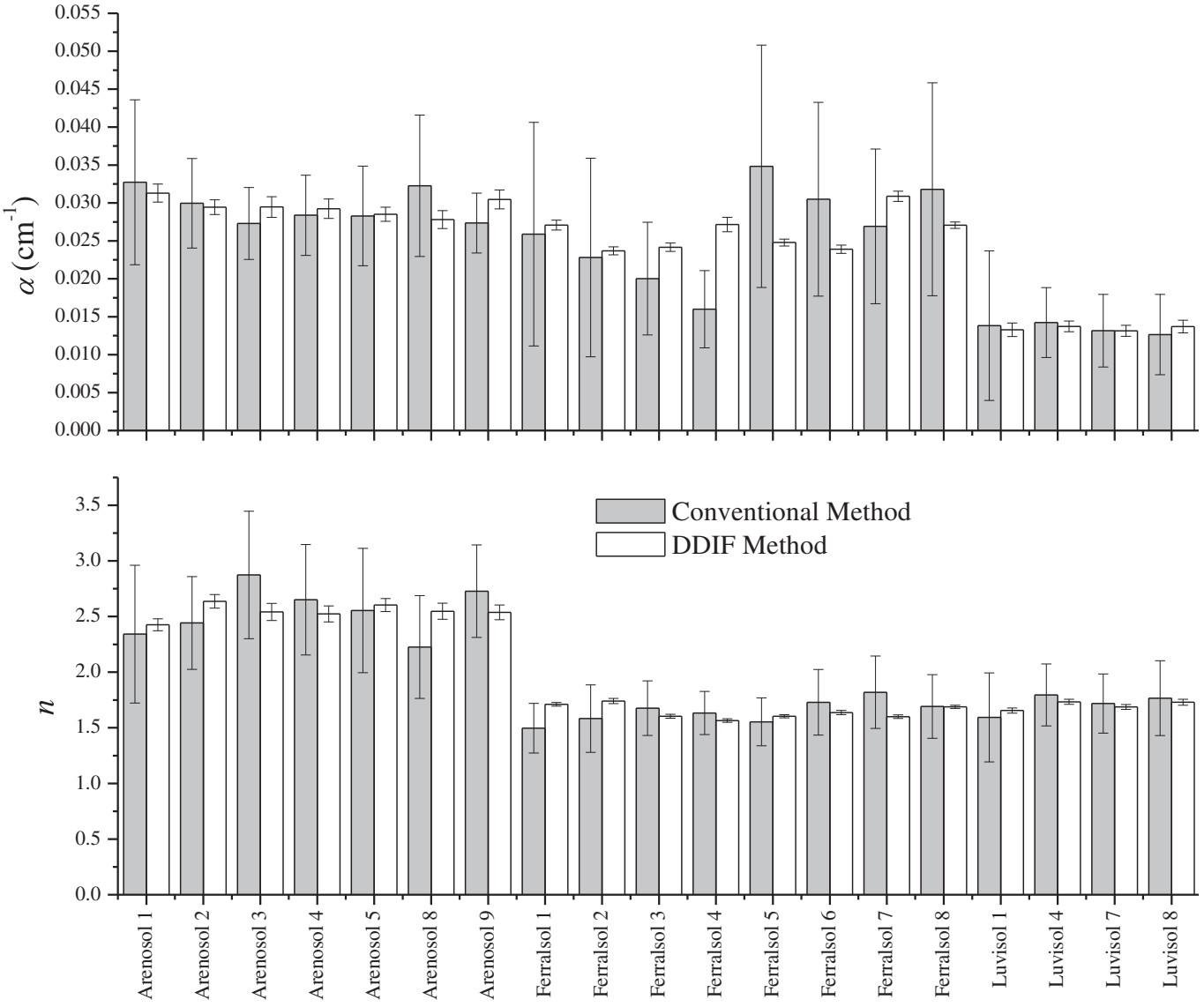

Fig. 10. Adjusted van Genuchten parameters from SWRC obtained by the conventional (tension table and pressure plate extractor) and DDIF methods after the shift of the matric potential (the minimum matric potential in the DDIF experiment for the Arenosol was ψ = -1,000 cm), the bars are the 95 % Confidence Intervals of the fitted parameters.

Empirically, the lower sand content of Luvisol (570 g kg^{-1}) than the soils studied using conventional T_1 or T_2 relaxation measurements (e.g., Costabel and Yaramanci, 2013) and; the broad pore size distributions and multiple pore size classes of the studied soils, which makes them unsuitable for the numerical method proposed by Müller-Petke et al. (2015) and Costabel et al. (2018), proved the wider applicability of the proposed method.

The existence of internal magnetic field gradients is the core of the DDIF method and it might be especulated that the method is resctrited to samples with large content of magnetic (or paramagnetic) impurities. However, while the presence of magnetic impurities in the surfaces of the pores is an important source of internal magnetic field gradients, the difference in the magnetic susceptibility in solid-liquid interfaces are also a source of internal gradients. Thus, even at low concentrations of magnetic impurities, the solid-liquid interface at the pore's walls may be a source of internal magnetic field gradient, which makes it possible to use DDIF (Song, 2003).

For instance, Liu et al. (2014) successfully applied DDIF to characterise limestone rocks and Song (2003) validated his proposal in Berea sandstone, both with a small density of paramagnetic impurities at the pore surface. Furthermore, the calibration and validation of the method are usually done in synthetic porous samples, such as randomly packed glass beds (Song, 2003; de Pierri et al., 2022), also with very low paramagnetic impurities and low magnetic susceptibility.

Besides that, one should also argue that the magnetic susceptibility differences scale up with the magnetic field and, consequently, can be enhanced in experiments performed at higher magnetic fields. However, in samples where DDIF could be not applicable, T_2 NMR relaxometry may be the method of choice. Indeed, concerning the evaluation of SWRC parameters, we do not see DDIF and T_2 NMR relaxometry as competing, but as complementary methodologies. In samples with a low concentration of paramagnetic impurities the use of DDIF would be more difficult, although the use of DDIF is usual in samples with low content of paramagnetic impurities (e.g., sandstone and carbonate rocks, glass beads). In fact, this paper extended the applicability of the method to samples with much higher paramagnetic impurities and magnetic susceptibility than usually in the literature, evidenced by the short encoding time (t_e). To do so, we chose challenging samples (low sand content and high paramagnetic impurities) to demonstrate the new approach.

Another point worthy of discussion is that, according to Song et al. (2003), a more precise evaluation of the pore size distribution using the DDIF approach requires that the internal magnetic field gradient (ΔB_z^i) distribution be linearly dependent on the pore sizes. Although this condition is somewhat expected to be fulfilled for more homogenous materials, in heterogeneous systems such as soil samples it is not trivial to guarantee such characteristics. However, the very good agreement between the SWRC obtained by the conventional method and the proposed one (Fig. 5 and Fig. S3) shows that, if present, the non-linearity between the internal magnetic field gradients and the pore sizes is not so significant to avoid a good prediction of the SWRC parameters. Nonetheless, more specifically, in-depth studies involving the comparison of the pore size distribution profiles obtained from other methods and DDIF are very welcome to verify to what extent the linear dependence of ΔB_z^i with the pore size is valid in soil samples, which may be important to increase the applicability of DDIF. Some studies in this direction are being carried out.

As a final remark, it is important to mention that to obtain an accurate and precise determination of the soil pore size distribution and the SWRC, it is important to follow a systematic experimental procedure for the sample preparation, execution of the experiments, and data processing. Given that the procedure described in the last section of the materials and methods was followed as guidance for the general execution of this type of analysis.

6. Conclusions

We have successfully demonstrated the use of the internal magnetic field modulation at Low Field ^{1}H NMR to access the high eigenmodes of diffusion using the Decay due to Diffusion in Internal Field (DDIF) method and estimate the pore size distribution, as well as the soil water retention curves. For this, we overcame the critical limitation of former NMR methods which is the need to estimate the surface relaxivity or calibrate the NMR results by support methods. Furthermore, the proposed method works well for complex undisturbed soils with sand contents as low as 57 wt%, surpassing the former proposals. We expect that this method will be efficient for measuring and estimating these hydro-physical attributes in other soils, however, further research is needed to confirm this. When compared with the conventional SWRC method, using tension tables and pressure plates, the proposed method is quicker (less than two hours when compared with weeks or even months of the conventional method), convenient and provides a higher resolution in the pore size distribution function. This method provided similar parameters to the van Genuchten model for the studied soils and is free of the errors and biases common to the conventional suction/pressure method. Although further research is needed for other soil classes with contrasting hydro-physical attributes, the proposed method shows good potential to substitute the expensive and difficult-to-maintain pneumatic systems.

Declaration of Competing Interest

The authors declare that they have no known competing financial interests or personal relationships that could have appeared to influence the work reported in this paper.

Data availability

Data will be made available on request.

Acknowledgements

We thank Stephan Costabel, one of the assignment reviewers, for the insightful comments, which in our opinion greatly improved the quality and significance of the manuscript. The corresponding author is especially grateful for the competent, constructive, cordial and kind review of Stephan Costabel. The authors acknowledge the support of the Financiadora de Estudos e Projetos (FINEP, 01.22.0081.00) and Council for Scientific and Technological Development, Brazil (CNPq, 430176/2018-0). Novotny E. H. acknowledges the Fundação de Amparo à Pesquisa do Estado do Rio de Janeiro, Brazil (FAPERJ, E_26/202.874/2018) and the Council for Scientific and Technological Development, Brazil (CNPq, 309391/2020-2). Cooper M. and Godoy G. acknowledge the Council for Scientific and Technological Development, Brazil (CNPq) and the Coordination for the Improvement of Higher Education Personnel (CAPES) for the fellowship and scholarship, respectively. deAzevedo E. R. thanks Brazilian Agencies FAPESP (Grants 2017/24465-3 and 2009/18354-8) and CNPq (Grant 303753/2018-8). Liu H. is thanked for the fruitful discussion. This work is part of Godoy G. MSc dissertation presented to the Soil and Plant Nutrition Graduate Program of ESALQ/USP.

Appendix A. Supplementary data

Supplementary data to this article can be found online at https://doi.org/10.1016/j.geoderma.2023.116363.

References

Bartoli, F., Philippy, R., Burlin, G., 1992. Influence of organic matter on aggregation in Oxisols rich in gibbsite or in goethite. I. Structures: the fractal approach. Geoderma 54, 231–257. https://doi.org/10.1016/0016-7061(92)90107-I.

Benavides, F., Leiderman, R., Souza, A., Carneiro, G., Bagueira, R., 2017. Estimating the surface relaxivity as a function of pore size from NMR T_2 distributions and micro-tomographic images. Comput. Geosci. 106, 200–208. https://doi.org/10.1016/j.cageo.2017.06.016.

Benavides, F., Leiderman, R., Souza, A., Carneiro, G., Azeredo, R.B.V., 2020. Pore size distribution from NMR and image based methods: A comparative study. J. Pet. Sci. Eng. 184, 106321 https://doi.org/10.1016/j.petrol.2019.106321.

Bittelli, M., Flury, M., 2009. Errors in water retention curves determined with pressure plates. Soil Sci. Soc. Am. J. 73, 1453–1460. https://doi.org/10.2136/sssaj2008.0082.

Brewer, ROY, 1965. Fabric and mineral analysis of soils. Soil Science 100 (1), 73.

Brownstein, K.R., Tarr, C.E., 1979. Importance of classical diffusion in NMR studies of water in biological cells. Phys. Rev. A. 19, 2446–2453. https://doi.org/10.1103/PhysRevA.19.2446.

Campbell, G.S., 1988. Soil water potential measurement: An overview. Irrig. Sci. 9, 265–273. https://doi.org/10.1007/BF00296702.

Campbell, G.S., Smith, D.M., Teare, B.L., 2007. In: Springer Proceedings in PhysicsExperimental Unsaturated Soil Mechanics. Springer Berlin Heidelberg, Berlin, Heidelberg, pp. 71–77.

Chen, P., Liu, J., Wei, C., Xue, W., Tian, H., 2017. Approach to rapidly determining the water retention curves for fine-grained soils in capillary regime based on the NMR technique. J. Eng. Mech. 143, 1–7. https://doi.org/10.1061/(ASCE)EM.1943-7889.0001231.

Costabel, S., Hiller, T., 2021. Soil hydraulic interpretation of nuclear magnetic resonance measurements based on circular and triangular capillary models. Vadose Zone J. 20, e20104.

Costabel, S., Weidner, C., Müller-Petke, M., Houben, G., 2018. Hydraulic characterisation of iron-oxide-coated sand and gravel based on nuclear magnetic resonance relaxation mode analyses. Hydrol. Earth Syst. Sci. 22, 1713–1729. https://doi.org/10.5194/hess-22-1713-2018.

Costabel, S., Yaramanci, U., 2013. Estimation of water retention parameters from nuclear magnetic resonance relaxation time distributions. Water Resour. Res. 49, 2068–2079. https://doi.org/10.1002/wrcr.20207.

Day, I.J., 2011. On the inversion of diffusion NMR data: Tikhonov regularization and optimal choice of the regularization parameter. J. Magn. Reson. 211, 178–185. https://doi.org/10.1016/j.jmr.2011.05.014.

de Pierri, L., Novotny, E.H., Cerri, C.E.P., de Souza, A.J., Mattos, B.B., Tornisielo, V.L., Regitano, J.B., 2022. Accessing biochar's porosity using a new low field NMR approach and its impacts on the retention of highly mobile herbicides. Chemosphere 287, 132237. https://doi.org/10.1016/j.chemosphere.2021.132237.

Dettmann, U., Bechtold, M., Frahm, E., Tiemeyer, B., 2014. On the applicability of unimodal and bimodal van Genuchten-Mualem based models to peat and other organic soils under evaporation conditions. J. Hydrol. 515, 103–115. https://doi.org/10.1016/j.jhydrol.2014.04.047.

Dlugosch, R., Günther, T., Müller-Petke, M., Yaramanci, U., 2013. Improved prediction of hydraulic conductivity for coarse-grained, unconsolidated material from nuclear magnetic resonance. Geophysics 78 (4), EN55–EN64.

Ghanbarian, B., Hunt, A.G., 2017. Improving unsaturated hydraulic conductivity estimation in soils via percolation theory. Geoderma. 303, 9–18. https://doi.org/10.1016/j.geoderma.2017.05.004.

Ghanbarian, B., Hunt, A.G., Daigle, H., 2016. Fluid flow in porous media with rough pore-solid interface. Water Resour. Res. 52, 2045–2058. https://doi.org/10.1002/2015WR017857.

Grebenkov, D.S., 2008. Laplacian eigenfunctions in NMR. I. A numerical tool. Concepts Magn. Reson. Part A Bridg. Educ. Res. 32, 277–301. https://doi.org/10.1002/cmr.a.20117.

Hansen, C., 1992. Analysis of discrete ill-posed problems by means of the L-curve. Soc. Ind. Appl. Math. 34, 561–580. https://doi.org/10.1137/1034115.

Holz, M., Heil, S.R., Sacco, A., 2000. Temperature-dependent self-diffusion coefficients of water and six selected molecular liquids for calibration in accurate ^{1}H NMR PFG measurements. Phys. Chem. Chem. Phys. 2, 4740–4742. https://doi.org/10.1039/b005319h.

Hunt A., Ewing R., 2009. Percolation Theory for Flow in Porous Media, second ed., Lect. Notes Phys. 771. Springer, Berlin Heidelberg. doi: 10.1007/978-3-540-89790-3.

IUSS Working Group WRB, 2015. World Reference Base for Soil Resources 2014, update 2015. International soil classification system for naming soils and creating legends for soil maps. World Soil Resources Reports N°. 106. FAO, Rome.

Jaeger, F., Bowe, S., Van As, H., Schaumann, G.E., 2009. Evaluation of ^{1}H NMR relaxometry for the assessment of pore-size distribution in soil samples. Eur. J. Soil Sci. 60, 1052–1064. https://doi.org/10.1111/j.1365-2389.2009.01192.x.

Jury, W.A., Horton, R., 2004. Soil Physics, 6th ed. Wiley, New York.

Keating, K., 2014. A laboratory study to determine the effect of surface area and bead diameter on NMR relaxation rates of glass bead packs. Near Surf. Geophys. 12, 243–254. https://doi.org/10.3997/1873-0604.2013064.

Keating, K., Knight, R., 2010. A laboratory study of the effect of Fe(II)-bearing minerals on nuclear magnetic resonance (NMR) relaxation measurements. Geophysics. 75, F71–F82. https://doi.org/10.1190/1.3386573.

Keating, K., Walsh, D.O., Grunewald, E., 2020. The effect of magnetic susceptibility and magnetic field strength on porosity estimates determined from low-field nuclear magnetic resonance. J. Appl. Geophy. 179, 104096 https://doi.org/10.1016/j.jappgeo.2020.104096.

Klute, A., 1986. Water retention: laboratory methods. In: Klute, A. (Ed.), Methods of Soil Analysis, Part I. Physical and Mineralogical Methods-Agronomy Monograph no, 9, second ed. American Society of Agronomy-Soil Science Society of America, Madison, pp. 635–662.

Knight, R., Walsh, D.O., Butler Jr., J.J., Grunewald, E., Liu, G., Parsekian, A.D., Reboulet, E.C., Knobbe, S., Barrows, M., 2016. NMR logging to estimate hydraulic conductivity in unconsolidated aquifers. Groundwater 54, 104–114. https://doi.org/10.1111/gwat.12324.

Kuncoro, P.H., Koga, K., Satta, N., Muto, Y., 2014. A study on the effect of compaction on transport properties of soil gas and water. II: Soil pore structure indices. Soil Tillage Res. 143, 180–187. https://doi.org/10.1016/j.still.2014.01.008.

Kutilek, M., Nielsen, D.R., 1994. Soil Hydrology. Catena Verlag, Cremlingen.

Levitt, M.H., 2001. Spin Dynamics: Basics of Nuclear Magnetic Resonance. John Wiley & Sons, Chichester.

Lisitza, N.V., Song, Y.-Q., 2001. The behavior of diffusion eigenmodes in the presence of internal magnetic field in porous media. J. Chem. Phys. 114, 9120–9124. https://doi.org/10.1063/1.1368659.

Liu, H., Nogueira, M., Obruchkov, S., Galvosas, P., 2014. Determining pore length scales and pore surface relaxivity of rock cores by internal magnetic fields modulation at 2 MHz NMR. J. Magn. Reson. 246, 110–118. https://doi.org/10.1016/j.jmr.2014.07.005.

Lourenco, S.D.N., Gallipoli, D., Augarde, C.E., Toll, D.G., Fisher, P.C., Congreve, A., 2012. Formation and evolution of water menisci in unsaturated granular media. Geotechnique. 62, 1143–1144. https://doi.org/10.1680/geot.12.D.004.

Luo, Z.-X., Paulsen, J., Song, Y.-Q., 2015. Robust determination of surface relaxivity from nuclear magnetic resonance DT_2 measurements. J. Magn. Reson. 259, 146–152. https://doi.org/10.1016/j.jmr.2015.08.002.

Medici, G., West, L.J., Banwart, S.A., 2019. Groundwater flow velocities in a fractured carbonate aquifer-type: Implications for contaminant transport. J. Contam. Hydrol. 222, 1–16. https://doi.org/10.1016/j.jconhyd.2019.02.001.

Meyer, M., Buchmann, C., Schaumann, G.E., 2018. Determination of quantitative pore-size distribution of soils with ^{1}H NMR relaxometry. Eur. J. Soil Sci. 69, 393–406. https://doi.org/10.1111/ejss.12548.

Müller-Petke, M., Dlugosch, R., Lehmann-Horn, J., Ronczka, M., 2015. Nuclear magnetic resonance average pore-size estimations outside the fast-diffusion regime. Geophysics. 80, D195–D206. https://doi.org/10.1190/GEO2014-0167.1.

Nimmo, J.R., 2009. Vadose Water. In: Likens, G.E. (Ed.), Encyclopedia of Inland Waters, 1. Elsevier, Oxford, pp. 766–777. https://doi.org/10.1016/B978-012370626-3.00014-4.

Rabot, E., Wiesmeier, M., Schlüter, S., Vogel, H.J., 2018. Soil structure as an indicator of soil functions: A review. Geoderma. 314, 122–137. https://doi.org/10.1016/j.geoderma.2017.11.009.

Ramos, P.F.O., de Toledo, I.B., Nogueira, C.M., Novotny, E.H., Vieira, A.J.M., Azeredo, R.B.V., 2009. Low field ^{1}H NMR relaxometry and multivariate data analysis in crude oil viscosity prediction. Chemom. Intell. Lab. Syst. 99, 121–126. https://doi.org/10.1016/j.chemolab.2009.08.001.

Rieu, M., Sposito, G., 1991. Fractal Fragmentation, Soil Porosity, and Soil Water Properties: I. Theory. Soil Sci. Soc. Am. J. 55, 1231–1238. https://doi.org/10.2136/sssaj1991.03615995005500050006x.

Santos, H.G., Jacomine, P.K.T., Anjos, L.H.C., Oliveira, V.A., Lumbreras, J.F., Coelho, M.R., Almeida, J.A., Araujo Filho, J.C., Oliveira, J.B., Cunha, T.J.F., 2018. Brazilian Soil Classification System, 5th ed. Embrapa, Brasília.

Schaumann, G.E., Hobley, E., Hurraß, J., Rotard, W., 2005. H-NMR relaxometry to monitor wetting and swelling kinetics in high-organic matter soils. Plant Soil. 275, 1–20. https://doi.org/10.1007/s11104-005-1708-7.

Simms, P.H., Yanful, E.K., 2001. Measurement and estimation of pore shrinkage and pore distribution in a clayey till during soil-water characteristic curve tests. Can. Geotech. J. 38, 741–754. https://doi.org/10.1139/cgj-38-4-741.

Solone, R., Bittelli, M., Tomei, F., Morari, F., 2012. Errors in water retention curves determined with pressure plates: Effects on the soil water balance. J. Hydrol. 470–471, 65–74. https://doi.org/10.1016/j.jhydrol.2012.08.017.

Song, Y.-Q., 2003. Using internal magnetic fields to obtain pore size distributions of porous media. Concepts Magn. Reson. Part A Bridg. Educ. Res. 18A, 97–110. https://doi.org/10.1002/cmr.a.10072.

Song, Y.-Q., Ryu, S., Sen, P.N., 2000. Determining multiple length scales in rocks. Nature. 406, 178–181. https://doi.org/10.1038/35018057.

Stingaciu, L.R., Weihermller, L., Haber-Pohlmeier, S., Stapf, S., Vereecken, H., Pohlmeier, A., 2010. Determination of pore size distribution and hydraulic properties using nuclear magnetic resonance relaxometry: A comparative study of laboratory methods. Water Resour. Res. 46, 1–11. https://doi.org/10.1029/2009WR008686.

Sucre, O., Pohlmeier, A., Miniere, A., Blümich, B., 2011. Low-field NMR logging sensor for measuring hydraulic parameters of model soils. J. Hydrol. 406, 30–38. https://doi.org/10.1016/j.jhydrol.2011.05.045, 2011.

Sun, W., Cui, Y., 2020. Determining the soil-water retention curve using mercury intrusion porosimetry test in consideration of soil volume change. J. Rock Mech. Geotech. Eng. 12, 1070–1079. https://doi.org/10.1016/j.jrmge.2019.12.022.

Sun, H., Lee, J., Chen, X., Zhuang, J., 2020. Estimating soil water retention for wide ranges of pressure head and bulk density based on a fractional bulk density concept. Sci. Rep. 10, 16666. https://doi.org/10.1038/s41598-020-73890-8.

Tadimalla S., Momot K.I., 2014. Effect of partial H_2O-D_2O replacement on the anisotropy of transverse proton spin relaxation in bovine articular cartilage. PLoS ONE 9(12): e115288. doi: 10.1371/journal.pone.0115288.

Teal, P.D., Eccles, C., 2015. Adaptive truncation of matrix decompositions and efficient estimation of NMR relaxation distributions. Inverse Problems 31 (4), 045010.

Topp G.C., Zebchuk W. 1979. The determination of soil water desorption curves for soil cores. Can. J. Soil Sci. 59, 19-26. doi: 10.4141/cjss79-003.

Tuller, M., Or, D., 2004. Water retention and characteristic curve. In: Hillel, D. (Ed.), Encyclopedia of Soils in the Environment, volume 4. Elsevier, Oxford, pp. 278–289. https://doi.org/10.1016/B0-12-348530-4/00376-3.

van Genuchten M.Th., 1980. A closed-form equation for predicting the hydraulic conductivity of unsaturated soils. Soil Sci. Soc. Am. J. 44, 892–898. doi: 10.2136/sssaj1980.03615995004400050002x.

Villarreal, R., Lozano, L.A., Polich, N.G., Salazar, M.P., Bellora, G.L., Turinetto, M.J., Soracco, C.G., 2020. Influence of soil water holding and transport capacity on glyphosate dynamics in two agricultural soils from Pampas Region. Geoderma. 376, 114566 https://doi.org/10.1016/j.geoderma.2020.114566.

Wang, T., Franz, T.E., Zlotnik, V.A., 2015. Controls of soil hydraulic characteristics on modeling groundwater recharge under different climatic conditions. J. Hydrol. 521, 470–481. https://doi.org/10.1016/j.jhydrol.2014.12.040.

Whittall, K.P., Bronskill, M.J., Henkelman, R.M., 1991. Investigation of analysis techniques for complicated NMR relaxation data. J. Magn. Reson. 95, 22l–l. https://doi.org/10.1016/0022-2364(91)90213-D.

Yu, Z., Zhang, Y., Xiao, L., Liao, G., 2019. Characterization of porous media by T_2–T_2 correlation beyond fast diffusion limit. Magn. Reson. Imaging. 56, 19–23. https://doi.org/10.1016/j.mri.2018.10.008.